

Multi-functional Coating for Icephobic Surfaces

Frederick Dynys (NASA-GRC), Eric Kreeger (NASA-GRC) & Alp Sehirlioglu (CWRU)

Abstract

Icing has been a technological challenge for aeronautical safety for decades. Current de-icing methods consume energy, utilize environmentally toxic fluids and expensive. Surface coatings that delay and/or reduce the accumulation of wet snow, ice, or frost is actively sought. Zinc oxide (ZnO) coatings were deposited on silicon substrates by a two-step process. The crystal structure, surface morphology and water contact angle (WCA) were measured by X-ray diffraction (XRD), scanning electron microscopy (SEM) and surface goniometry. Seed layer and ZnO precursors were investigated; both had a large impact on ZnO morphology and wetting behavior. Depending upon the processing conditions, the WCA varied from 8° to 147° . Highest WCAs were achieved using surface assisted monolayer (SAM) of stearic acid (147°), ZnO etching (130°) and carbon nano-tube seed layer (129°). A super-hydrophobic surface ($>150^\circ$) was not achieved. Water droplets were highly adherent to the ZnO coating, exhibiting no motion or rolling upon tilting; undesirable property for inhibiting ice formation.

Introduction

Prevention of icing has been a technological challenge for decades to increase the safety level for aircraft exposed to atmospheric icing environments. Ice distorts the aerodynamic flow which adversely affects aircraft handling and significantly increases drag. De-icing methods have been developed based on mechanical or thermal energy concepts. These methods are proven but consume a great deal of energy and/or necessitate elaborate infrastructures and maintenance.

Ice accretion on aircraft surfaces occurs by droplet/substrate collision followed by freezing. Approach to mitigate icing has been inspired by super hydrophobic (SH) surface technology utilized by nature to bead water droplets. Historically, hydrophobic materials have failed to mitigate icing. The problem with most surfaces is that water droplets adhere to the surface upon impact. SH surfaces have unique properties that shed water droplets by droplet recoil upon impact and droplet motion at low incline angles ($<5^\circ$). Shedding properties are dependent upon droplet size, temperature and impact velocity. SH surface aids in ice prevention and reduces ice/substrate interfacial bond strength. SH surfaces do not equate to icephobic surface. Mishchenko et al.¹ reported icing on SH surfaces at $<-25^\circ\text{C}$. SH structures also fail to prevent ice accretion from vapor condensation, demonstrated by Varanasi et al.² Additionally, high velocity impact of water droplets during flight can cause water penetration into the SH structure, transforming the surface to hydrophilic state. Once ice accretion occurs on SH surface, the surface is incapable of repelling ice growth.

Interfacial bonding between ice and substrate can be mitigated by electrolysis. The polar nature of the water molecule influences the freezing temperature. There are a number of studies since 1861 indicate that the local electric field near charged surfaces may enhance the freezing of supercooled water, so-called electrofreezing. Pioneer work by Petrenko and Qi³ discovered that application of a low DC current ($\sim 1 \text{ mA/cm}^2$) at an interface comprised of a fine matrix of electrodes can depress freezing point. Petrenko has shown that AC fields are more effective in ice mitigation than DC field because electrical conductivity of ice is enhanced at higher frequency; AC reduces power consumption ($<1 \text{ KW/m}^2$) compared to joule heating (30-40

KW/m²) required for melting ice. Additionally, surface charge generated by pyroelectric materials can enhanced and depressed the freezing point of water by ± 5.5 °C.⁴ Surface treated piezoelectric ZnO nanorods has been observed to delay water freezing by 90 minutes.¹ These observations clearly demonstrate the importance of electric charge/field on ice prevention.

This preliminary investigation reports on the feasibility is to develop icephobic surface by *designing a functional piezoelectric electric material into a super hydrophobic structure*. This integration improves icing technology by providing multiple mechanisms to prevent icing. The role of the SH structure is to shed water droplets. Electrical approach mitigates ice bonding to substrate either by freezing point depression and/or electrolysis. This phase I approach investigated self power generation by piezoelectric ZnO fibers, where electrical generation is driven by structural vibrations and acoustic noise.

Experimental Procedure

Fabrication of nanostructure ZnO was done by aqueous chemical bath deposition (CBD) at atmospheric pressure. ZnO CBD is based on the reaction involving dissolved Zn⁺² ions and urea (hexamethylenetetramine-HMTA). Analytical grade salts were used in the CBD process

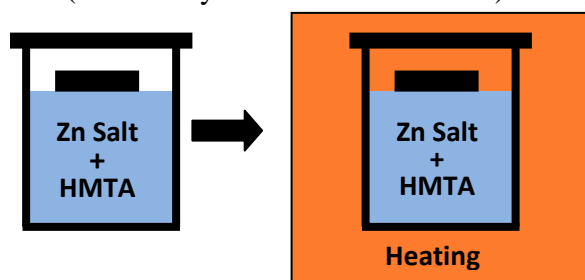


Figure 1 - ZnO growth process.

without further purification. A ZnO seed layer was deposited on the substrates prior to CBD process; the layer acts as heterogeneous nucleation site for ZnO growth. Figure 1 illustrates the overall CBD process. A 250 ml Teflon vessel was charged with the reactants and silicon wafer was suspended on top of the solution. The vessel top was not fully tighten to allow venting of excess pressure. The charged vessel was placed in pre-heated oven set at 90 °C

for typical time period of 4 hrs. The oven is programmable. Once the process time period expired, it returned to room temperature at uncontrolled cooling rate. Samples were withdrawn from the vessel, carefully rinsed in DI water to avoid coating damage and dried at 70-90 °C in air.

Table 1

Seed Layer	Substrate	Zn Salt	Hydrolysis	T (°C)	Time (Hrs)	HMTA/Zn Ratio
Colloidal ZnO	Si	Zn Nitrate	HMTA	90	4	1
ZnO via Zn Acetate	Si	Zn Nitrate	HMTA	90	4	1
PVD ZnO	Si	Zn Nitrate Zn Chloride Zn Acetate	HMTA	90	4, 14 72	1, 1.25, 1.5, 2, 3
Colloidal Ag	Si	Zn Nitrate	HMTA	90	4	1
PVD Ag	Si	Zn Nitrate	HMTA	90	4	1
Carbon Nanotubes	Si	Zn Nitrate	HMTA	90	4	1
PVD Zn	Si	Zn Nitrate	HMTA	90	4	1
Colloidal ITO	Si	Zn Nitrate	HMTA	90	4	1
None	Al	Zn Nitrate	HMTA	90	4	1

Growth of ZnO films were achieved primarily on commercially polished Silicon substrates. Silicon substrates were cleaned with either ethanol or acetone prior to seed layer deposition. Table I shows overview of varied process parameters. The practical requirements for ZnO synthesis are morphology control, size, crystallographic orientation and particle density. We began with recipes known to produce nano-rods and proceeded to adjust the process based upon characterization feedback. Seed layer, Zn salt, Zn salt concentration, HMTA/Zn ratio, pH and time were experimentally varied. Temperature and HMTA were kept constant. Ammonia hydroxide (0.01-0.04 M) and polyethyleneimine (0.001-0.01 M) were additives tried for growth control.

As shown in Table I, different seed layers were investigated. Oriented growth of ZnO nanorods was achieved using a ZnO seed layer deposited by physical vapor deposition (PVD). PVD was achieved utilizing radio frequency magnetron sputtering (Lesker PVD75). The chamber was evacuated down to the background pressure of 3×10^{-5} Torr. Substrates were heated to 400 °C at heating rate of 10 °C/min. The chamber was backfilled with argon/oxygen (29 sccm Ar/34 sccm O₂) gas flow to achieve a process pressure 2×10^{-2} Torr. The ZnO target was sputtered at 8.9 W/cm². The target to substrate distance was about 13 cm. ZnO films were deposited at 5, 10, 20, 30 and 45 minutes. Based on the sample interference color, the deposition rate was estimated to be 2.7 nm/min.

Ag and Zn seed layers films were also deposited by PVD at room temperature. The chamber was evacuated down to the background pressure of 3×10^{-5} Torr and backfilled with argon to achieve a process pressure 2×10^{-2} Torr. The Zn and Ag targets were sputtered at 3.9 and 9.9 W/cm², respectively. Deposition time was varied from 1 to 5 minutes.

Substrates were also coated with a ZnO seeding layer by a sol-gel technique using colloidal suspension or ZnO precursor. Coating deposition was achieved by spin coating method at 1000-2000 rpm. Substrates were coated with 0.005 M Zn acetate(Aesar)/ethanol solution; coating step was repeated 3 to 5 times followed by thermal decomposition of the Zn acetate film at 250 °C for 10 min. Thicker ZnO films were achieved by repeating the above process. Colloidal suspensions were deposited using aqueous ZnO suspension(30-40 nm, 20 Wt.%, US Research Nanomaterials), ZnO (<35 nm, 40 wt.%, Aldrich) dispersed in ethanol, SnO₂ doped In₂O₃ (<100 nm, 30 wt.%, Aldrich) dispersed in isopropanol and aqueous Ag suspension (10 nm, 0.02 mg/ml in aqueous buffer, Aldrich). Alcohol improves the substrate wetting than aqueous system. Colloidal suspensions were diluted with appropriate liquid (water or alcohol) to control the particle density.

The ZnO morphology and size were characterized by Hitachi S-4700 field emission scanning electron microscope. ZnO crystallographic structure was characterized by x-ray diffraction (XRD) using Bruker D-8 Advance diffractometer (Cu K α radiation). Wetting contact angle (WCA) was measured using Ramè-Hart Model 590 Advanced Goniometer with DROPimage advanced V2.4 software. De-ionized water was used for WCA measurements. A 250 μ L syringe was used to generate the water droplet. A 2.5 μ L droplet was used to measure the static water contact angle (WCA) at room temperature; 3-5 measurements were performed to achieve average WCA.

Results and Discussion

The hydrolysis and condensation reactions of zinc salts result in one-dimensional ZnO crystal growth under a wide variety of conditions. In general, rod/wire growth is possible in

slightly acidic to basic conditions ($5 < \text{pH} < 12$) at temperatures from 50 to 200 °C. Wires are formed at $\text{pH} > 9$ in the absence of additives. Basic conditions are crucial because divalent metal ions do not readily hydrolyze in acidic media. For growth at $\text{pH} < 9$, additives such as HMTA are used to promote one-dimensional ZnO precipitation. HMTA slowly releases hydroxide ions by temperature-dependent hydrolysis. The amine based ligand complexes with Zn^{+2} ion to control crystal growth. Hydroxyl ions react with Zn ions to form hydrated ZnO. Substrates with seeded layers are utilized to selectively grow ZnO film at the substrate surface.

For heterogeneous growth, the seed layer reduces the super-saturation level needed for nucleation compared to homogeneous nucleation. This defines a concentration window for selective growth on the substrate. Different seed layers were utilized to control particle density, morphology, size and crystallographic orientation. Metallic seed layers were also pursued for bottom electrode for electrical characterization of ZnO nano-rods. Figure 2 shows the affect of the different seed layers on ZnO growth using similar process conditions. Non-oriented nano-rod growth, confirmed by x-ray diffraction (XRD), was observed for seed layers of colloidal ZnO (1 & 20 Wt.%), colloidal SnO_2 doped I_2O_3 (ITO 1% Wt.), Zn acetate, physical vapor deposited (PVD) Zn film, PVD Ag film, Colloidal Ag (1% Wt.) and carbon nanotubes (CNT) (Figs. 2A, 2B, 2D, 2E, 2G-2J). Ag, CNT and ITO seeded samples exhibited large rod diameters (1-2 μm), long rod lengths (6-10 μm), hexagonal morphology and rod density approximately $10^6/\text{cm}^2$. Smaller rod diameters (0.06-13 μm) and lengths ($\leq 2 \mu\text{m}$) were observed for Zn acetate, PVD Zn and colloidal ZnO seed layers. ZnO rods derived from Zn acetate and Zn metal exhibited a tapered morphology, whereas cylindrical morphology is observed from the colloidal ZnO seeds. Oriented rods were achieved by PVD of the ZnO seed layer, shown in Fig. 2C. XRD of the oriented ZnO rods on the Si substrate showed only the ZnO (002) peaks, indicating that growth direction is along the $\langle 0001 \rangle$ axis. The seed layer was deposited at 400 °C. Nano-rod diameters ranged from 0.06-1.3 μm with lengths $\leq 2 \mu\text{m}$. PVD seed layers were grown at 5, 10, 20, 30 and 45 minutes to control the nano-rod density. All samples exhibited similar nano-rod densities of $10^8 - 10^9/\text{cm}^2$.

PVD Ag layer resulted in a dual microstructure containing nano-rods and fibrillar ZnO as shown in Fig. 2E. ZnO growth on unseeded Al surface resulted in fibrillar microstructure with no nano-rods as shown in Fig. 2F.

Three different zinc salts were used for ZnO fabrication: 1) zinc nitrate ($\text{Zn}(\text{NO}_3)_2 \cdot 6\text{H}_2\text{O}$), 2) zinc chloride ($\text{ZnCl}_2 \cdot x\text{H}_2\text{O}$) and 3) zinc acetate ($\text{Zn}(\text{O}_2\text{C}_2\text{H}_3)_2$). All three salts at 0.025 M and identical seed layer (PVD ZnO) produced different microstructures as shown in Fig. 3. ZnCl_2 produced non-oriented ZnO rods that are 0.6-2 μm in diameter and lengths on the order of 8 μm . These ZnO rods also exhibited etching like behavior at the growth site. Outer shell is observed

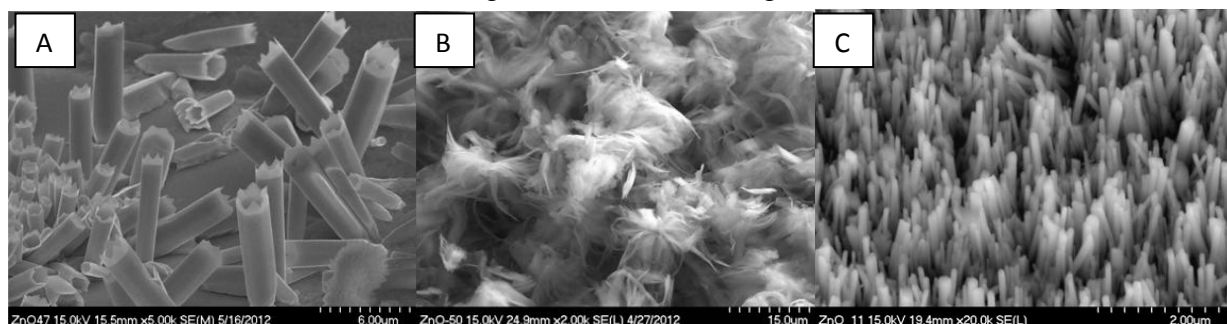


Figure 3 - ZnO microstructures derived from A) Zn Chloride, B) Zn Acetate and C) Zn Nitrate.

with a hollow interior; this is a good feature for hydrophobic structures by reducing the contact

area. $\text{Zn}(\text{O}_2\text{C}_2\text{H}_3)_2$ produced a fine fibrillar microstructure. Oriented ZnO nano-rods is produced by $\text{Zn}(\text{NO}_3)_2$; rod physical characteristics were reported earlier in the section. The observed trend is that ZnCl_2 produces larger diameter and longer ZnO rods. In terms of hydrophobicity, the trend is $\text{Zn}(\text{O}_2\text{C}_2\text{H}_3)_2 > \text{ZnCl}_2 > \text{Zn}(\text{NO}_3)_2$.

Table 2

Seed Layer	Zn Salt	Zn Conc.	HMTA/ Zn Ratio	Time Hrs	WCA	Comments
Zn Acetate	Zn Nitrate	0.025 M	1	4	147°	Stearic acid treated
PVD 20 min 400C	Zn Nitrate	0.05 M	1	4	130.1°	Etchant $\text{NH}_4(\text{OH})$
carbon nanotube	Zn Nitrate	0.025 M	1	4	128.9°	Mixed with Nanotube
PVD 20 min 400C	Zn Nitrate	0.05 M	1	4	127.5°	Etchant $\text{NH}_4(\text{OH})/\text{CTAB}$
Colloidal	Zn Nitrate	0.025 M	1	4	109.2	20 Wt. % ZnO
PVD 45 min 400C	Zn Acetate	0.025 M	1	4	106.7°	
PVD 20 min 400C	Zn Acetate	0.025 M	1	4	104.2°	
PVD 10 min 400C	Zn Nitrate	0.025 M	1.67	4	102.5°	

Table 2 shows the highest static WCAs achieved. It should be noted that these hydrophobic surfaces did not display a droplet roll off angle. Droplets adhered to the substrate at all orientations as shown in Fig. 4. Droplet adhesion is undesirable for abating ice formation.

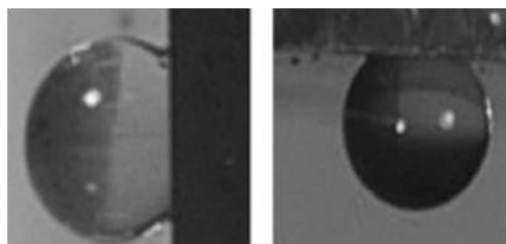


Figure 4. Droplet adhesion to substrate.

Post treatments were sought to promote hydrophobicity. The ZnO coating (Fig. 2E) treated with stearic acid (0.005M), self assembled monolayer (SAM), achieved the highest WCA of 147°. The initial WCA was 19° before treatment with stearic acid. WCA result is lower than Saleema and Farzaneh⁷. They reported WCA of 173.1° for stearic acid treated ZnO nano-rods; contact angle hysteresis (CAH) as low as 1.4°. However, the ZnO synthesis method differs from Saleema and Farzaneh; their synthesis method should be evaluated. Lin et al.⁸ achieved a WCA of 150° using SAM treatment of octadecyltrichlorosilane. A fluorinated SAM treatment was tried using

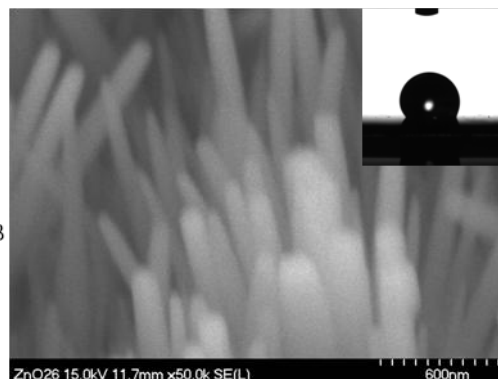
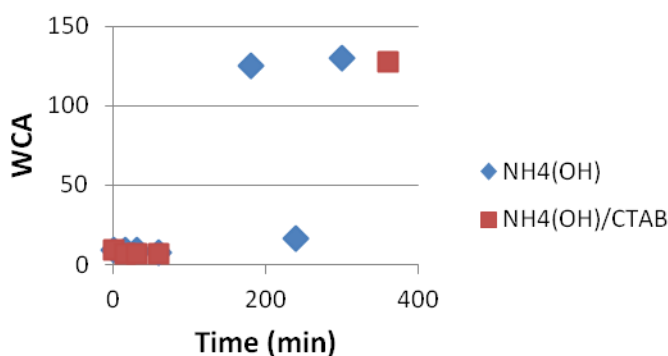


Fig. 5 WCA as function of etch time. SEM photograph of etched ZnO nano-rods.

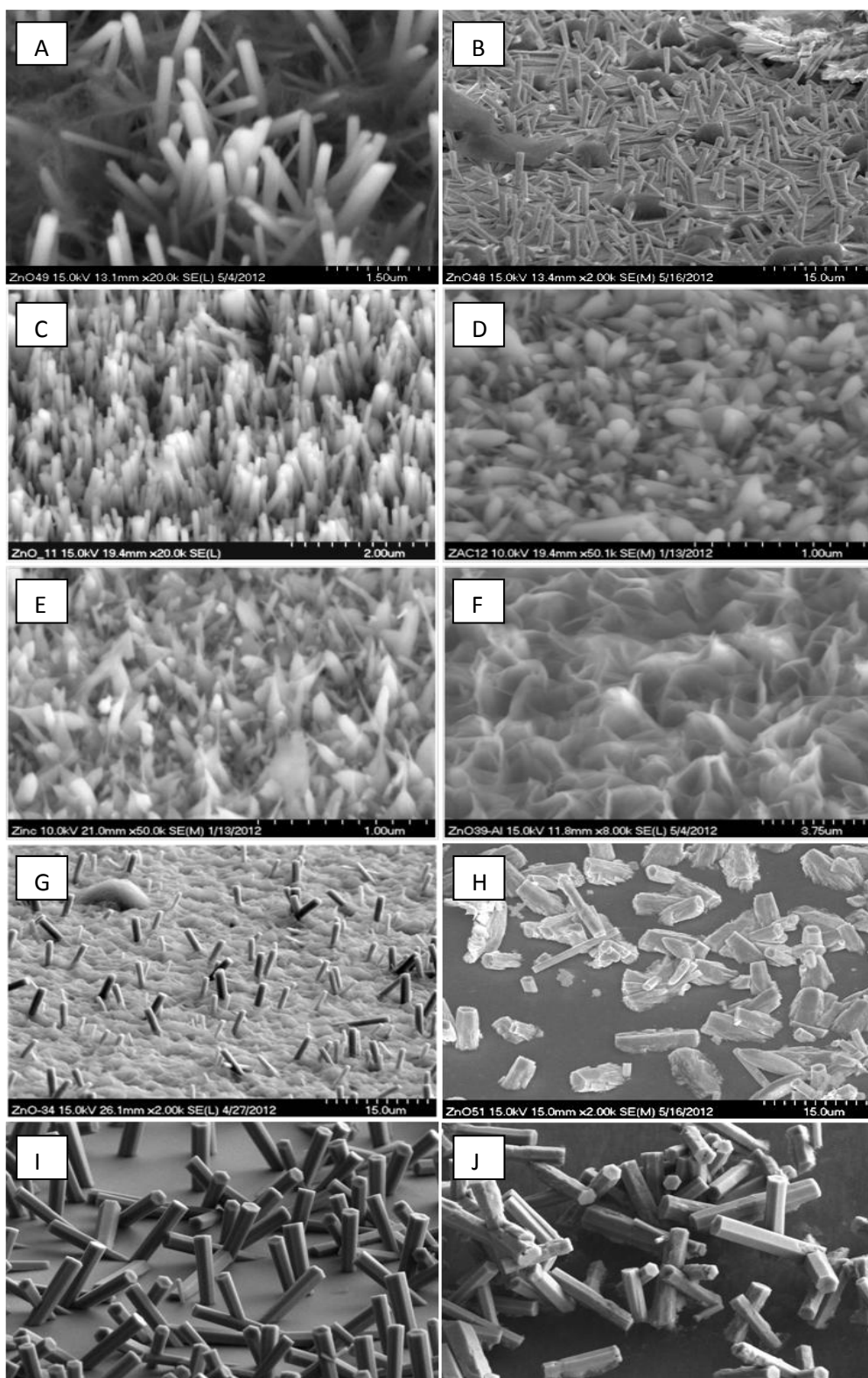


Fig. 2 Seed layer affect on ZnO morphology A) colloidal ZnO, B) Colloidal ITO, C) PVD ZnO, D) PVD Zn, E) Zn Acetate, F) non-seeded Al surface, G) PVD Ag, H) Colloidal Ag, I) CNT substrate, J) CNT.

heptadecafluoro-1,1,2,2-tetrahydrodecyl-triethoxysilane; WCA of 126.1° was achieved. Anisotropic etching of the ZnO nano-rods based on reported etchants^{9,10}. Etching ZnO nano-rods with $0.14\text{M NH}_4(\text{OH})$ and $0.29\text{M NH}_4(\text{OH})/0.013\text{M Cetyl Triammonium Bromide (CTAB)}$ also transformed a hydrophilic surface (WCA 9.5°) to hydrophobic surface (127.5°) as shown in Figure 5. Microstructural observations indicated that the etching tapers the ZnO rods, reducing the contact area with the water droplet.

Silicon substrates coated with CNT by CVD were acquired from General Nano. The CNT forest was cleaved from the silicon substrates; a remnant CNT coating remained on the substrate. It was surprising that ZnO growth occurred on the CNT sample (Fig. 2J). The metallic catalyst used for CNT growth probably acted as a seed for ZnO growth. CNT samples exhibit static WCA of 143° . The growth of ZnO on CNT reduced the static WCA to 128.9° . None of the measured samples exhibit a droplet roll-off angle, droplet was strongly adherent to the coating.

The static WCAs in the $100\text{--}110^\circ$ range were achieved with Zn acetate and Zn nitrate salts. Zn nitrate combined with seed layer derived from aqueous dispersed ZnO (colloidal) produced WCA of 109.2° . Whereas, ethanol dispersed ZnO seed layer produced a hydrophilic surface (26.7°). There was no clear trend in the effect of HMTA/Zn ratios on WCA; one sample at 1.67

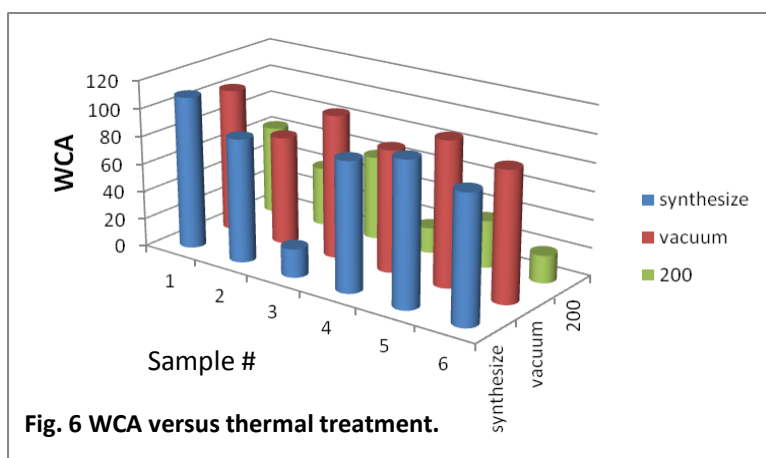


Fig. 6 WCA versus thermal treatment.

ratio exhibited WCA of 102.5° . In general, hydrophobic surfaces (WCA of $90\text{--}100^\circ$) occurred when the Zn nitrate concentration $<0.01\text{M}$.

Static WCAs were measured on thermally treated samples. Samples were thermally treated in vacuum at 100°C and air at 200°C . Barshilia et al.¹¹ achieved WCA of 155.2° by vacuum annealing ZnO coatings. The thermal treatments did not achieve a SH surface. Fig. 6

shows a sample of the effect of thermal treatments on WCA. Vacuum treatment enhanced the

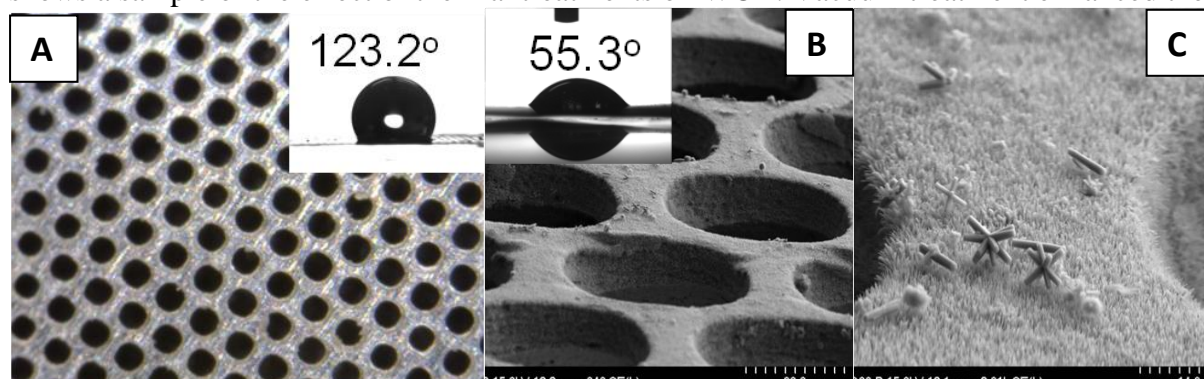


Fig. 7 A) Uncoated mesh; B & C) ZnO coated mesh.

WCA for sample 3, but it was non-effective for the other samples. Annealing in air at 200°C made the samples more hydrophilic (lower WCA); Saleema and Farzaneh also observed a reduction in WCA by annealing in air.

A double roughness scale was attempted to fabricate a SH surface. A etched stainless steel

mesh screen, 127 μm diameter hexagonal hole pattern, was acquired from Vacco Industries. The non-coated mesh exhibit a WCA of 127.3° . A ZnO seed layer was deposited on the mesh by

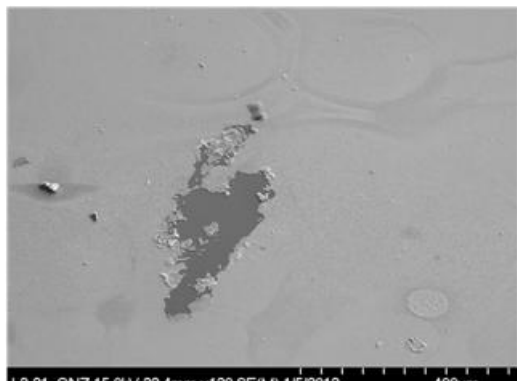


Fig. 8 Failed ZnO Coating.

PVD. ZnO nano-rods were grown on the mesh from Zn nitrate. Fig. 7 shows the microstructure of the ZnO coated stainless steel mesh. ZnO coating made the mesh hydrophilic, measure WCA was 55.3° .

Finally, the synthesized ZnO films had to be handled carefully. Rinsing the film or touching the surface was sufficient in damaging the ZnO film as shown in Fig. 8. Since the film porosity is needed for SH surface, strategies are required to improve the mechanical robustness without deteriorating hydrophobic nature.

Summary

Hierarchical ZnO films with random and preferred crystal orientation have been prepared by a simple two step deposition process on silicon substrates. PVD ZnO seed layer with Zn nitrate produced aligned and (0 0 2) orientated ZnO nano-rods. Random oriented ZnO rods structured films were also observed using Zn nitrate with seed layers fabricated from colloids, Zn Acetate and CNT. In addition to the seed layer, the Zn precursor affected the ZnO size and morphology: Zn acetate produced a fibrillar ZnO, Zn chloride produced non-orientated micron sized ZnO rods and Zn nitrate produced aligned and (0 0 2) orientated ZnO nano-rods.

There was no strong correlation between WCA and process. ZnO coatings exhibited hydrophilic to hydrophobic properties. SAM treatment and etching of ZnO coating achieved the highest WCAs (127° - 147°). Deposition on CNT coating also achieved a high WCA of 128.9° . However, the CNTs maybe controlling the wetting behavior. Other treatments such as thermal treatments, seed layer, Zn salt, Zn salt concentration, HMTA/Zn ratio, pH and time did not achieved super-hydrophobic coating. The fabricated hydrophobic coatings exhibit a strong adhesion to water droplets, ineffective for inhibiting ice formation.

References

- 1- Mishchenko et al., ACS Nano, 4, 7699, 2010.
- 2- Varanasi et al. Applied Physics Letters, 97, 234102, 2010
- 3- Petrenko, US Army report 39152.11-EV, 2003.
- 4- Ehre et al., www.sciencemag.org/cgi/content/full/327/5966/672/DC1
- 5- He et al., Soft Matter, 7, 3993, 2011.
- 6- Yu et al., ACS Nano, 5, 7885, 2011.
- 7- Saleema & Farzaneh, Applied Surface Science, 254, 2690, 2008.
- 8- Lin et al., Applied Surface Science 254, 7370, 2008.
- 9- Liu et al., Applied Surface Science 252, 8668, 2006.
- 10- Mehta & Meier, Journal of The Electrochemical Society, 158, H119, 2011.
- 11- Barshilia et al., Applied Surface Science 257, 4410, 2011.

